PCCP

Photodissociation of *p*-ethyl- and *p*-(α-hydroxyethyl)toluene in solution

M. Fujiwara* and K. Mishima

Graduate School of Science, Hiroshima University, Kagamiyama, Higashi-Hiroshima 739-8526, Japan

Received 22nd May 2000, Accepted 3rd July 2000
Published on the Web 9th August 2000

Photodissociation of *p*-ethyl- and *p*-(α-hydroxyethyl)toluene at 266 nm in *n*-heptane solution was studied by nanosecond fluorescence and absorption spectroscopy. *p*-Ethyltoluene dissociates by CH–H bond fission in the CH_2 group. *p*-(α-Hydroxyethyl)toluene decomposes by CH–OH bond fission in the CH(OH) group. The quantum yields are of the order of $\sim 10^{-3}$ for dissociation of *p*-ethyl- and *p*-(α-hydroxyethyl)toluene. For *p*-ethyltoluene, the dissociation rate of 4.0×10^7 s^{-1} is equal to the fluorescence decay rate of 4.0×10^7 s^{-1}. For *p*-(α-hydroxyethyl)toluene, the dissociation rate of $> 1.0 \times 10^9$ s^{-1} is much faster than the fluorescence decay rate of 4.5×10^7 s^{-1}. One-photon excitation is required for dissociation of *p*-ethyl- and *p*-(α-hydroxyethyl)toluene. A model is proposed to interpret the observations. For *p*-ethyltoluene, since the S_1 [ππ*(benzene)] state does not correlate adiabatically to the σσ*(C–H) state, intersystem crossing proceeds to the T_1 [ππ*(benzene)] state, which crosses to the σσ*(C–H) state, leading to CH–H bond fission. For *p*-(α-hydroxyethyl)toluene, the S_1 [ππ*(benzene)] state crosses adiabatically to the np(O)σ*(C–O) state, allowing rapid CH–OH bond fission.

1. Introduction

Photoexcitation of methyl-[1–12] and hydroxymethyl-substituted[10,11,13] aromatic molecules is known to induce, respectively, dissociation of the CH_2–H and CH_2–OH bonds yielding arylmethyl radicals. In the liquid phase (non-polar solution), the CH_2–H bond fission rate of *p*-methylanisole is equal to its fluorescence decay rate,[11] and the CH_2–OH bond fission rate of *p*-(hydroxymethyl)anisole is much faster than its fluorescence decay rate.[11] The observations show the existence of two distinct dissociation channels: CH_2–H bond fission *via* thermally equilibrated levels of the S_1 state and CH_2–OH bond fission from vibrationally excited levels of the S_1 state.

With respect to the thermally equilibrated S_1 states, the fluorescence lifetimes (~20 ns) of *p*-ethyltoluene (ET) and *p*-(α-hydroxyethyl)toluene (HET) are longer than those (~6 ns) of *p*-methylanisole and *p*-(hydroxymethyl)anisole, which are close to the time widths (~4 ns) of nanosecond laser pulses. The substituted toluenes are more suitable than the anisoles for studies on excited states that lead to dissociation.

The present paper deals with photodissociation of ET and HET at 266 nm in *n*-heptane solution. Fluorescence and absorption experiments with nanosecond time resolution were employed. For ET, CH–H bond fission takes place to produce an α, *p*-dimethylbenzyl (DMB) radical. For HET, CH–OH bond fission occurs to yield the same radical. The dissociation mechanisms of these molecules are discussed in terms of electronic coupling.

2. Experiment and simulation

ET (Tokyo Chemical, >95%) and HET (Tokyo Chemical, >96%) were distilled. *p*-(α-Chloroethyl)toluene (CET) was prepared by treatment of HET with oxalyl chloride in dry dichloromethane. It was separated by column chromatography on silica gel with chloroform as eluent and then distilled. Naphthalene (Nacalai Tesque) was recrystallized from ethanol. *n*-Heptane (Dojindo spectrosol) was used as received. The sample solutions, containing ET (4.9×10^{-3} mol dm^{-3}), HET (6.9×10^{-3} mol dm^{-3}), and CET (8.8×10^{-3} mol dm^{-3}) with *n*-heptane, were degassed by freeze–pump–thaw cycles prior to sealing in a 10 × 10 mm quartz cell.

For the nanosecond fluorescence measurement, a pulse of the fourth harmonic (266 nm, <0.5 ns rms jitter) of a Nd : YAG laser (Quanta-Ray GCR-11) was used as the photolysis light. A second pulse (308 nm) from a XeCl excimer laser (Lumonics 500) induced the fluorescence. The laser pulse fluences were attenuated with ND filters (Sigma FNDU-50C02-10, -20, -50) and measured with a thermopile monitor (Ophir 03A-P, DGX). The delay time was adjusted with a digital delay generator (EG&G PAR 9650, <0.1 ns rms jitter). The 266 and 308 nm laser beams were focused co-axially on the cell to 1.6 × 12.0 and 1.6 × 4.0 mm rectangular profiles, respectively. The fluorescence was collected into a monochromator (Ritsu MC-10N) at a right-angle to the laser beams and detected with a photomultiplier (Hamamatsu R636). Part of the 308 nm beam was directed on a PIN photodiode (Hamamatsu S1722-02). The output signals from both the photomultiplier and photodiode were fed simultaneously to separate channels of a digital oscilloscope (Tektronix 2440, 500 MHz sampling, <0.1 ns rms jitter), which was interfaced to a personal computer (NEC PC-9801UV) for data storage.

For the transient absorption measurement, the photolysis light was the 266 nm laser pulse. The white light was provided by a Xe arc lamp (Ushio UXL-500D-O). The laser and lamp beams were focused on the cell at right angles to each other to 1.6 × 12.0 mm rectangular and 1.6 mm circular profiles, respectively. The detection apparatus for the white light was the same as for the fluorescence. All experiments were performed at room temperature (~295 K).

The growth curve of the ground-state radical, observed as the dependence of its fluorescence intensity on the delay time

from the pump (266 nm) to the probe (308 nm) pulse, is reproduced by the following expression:

$$S(t) = F_{grow}(t) * I_{pump}(t) * I_{probe}(t). \quad (1)$$

The symbol * means convolution. $I_{pump}(t)$ and $I_{probe}(t)$ are the intensity–time profiles of the excitation pulses; their best forms are Gaussian functions with 4.5 and 4.0 ns widths (FWHM), respectively. $F_{grow}(t)$ is the population function of the ground-state radical:

$$F_{grow}(t) = 1 - \exp(-k_{grow}\, t), \quad (2)$$

where k_{grow} is the growth rate constant of the ground-state radical to be determined. The calculation is made with a 0.2 ns increment.

3. Results

3.1. Identification of dissociation product

In order to identify the fragment radical formed from photodissociation of ET and HET, the fluorescence and absorption spectra with nanosecond time resolution were measured.

The nanosecond fluorescence spectra, shown in Fig. 1, were observed by excitation with the 308 nm pulse after photolysis of ET, HET, and CET with the 266 nm pulse. Excitation with the 308 nm pulse alone did not induce the fluorescence. The three fluorescence spectra are identical within experimental error and exhibit a band at 500 nm. The fluorescence intensities decreased following a second-order decay process by increase of the delay from the 266 to the 308 nm pulse and disappeared at 100 μs. The fluorescence lifetimes, determined from photolysis of ET, HET, and CET, agree well and are a value of 103 ± 14 ns. The fluorescence spectra in Fig. 1 are assigned to the DMB radical, since it is the only product formed from the three molecules, and since substituted benzyl radicals are formed by C–X bond fission (X = Cl, Br).[6,9,10,14–16] Clearly, ET dissociates by CH–H bond fission to produce the DMB radical, and HET decomposes by CH–OH bond fission to yield the same radical. The fluorescence spectra of the DMB radical bear some resemblance to those of the benzyl[14] and *p*-methylbenzyl[14] radicals, but the fluorescence lifetimes of the DMB radical are definitely longer than those of the benzyl (<1 ns),[14] α-methylbenzyl (12 ns),[15] and *p*-methylbenzyl (14 ns)[14] radicals.

The transient absorption spectra, shown in Fig. 2, were recorded by excitation of ET, HET, and CET with the 266 nm pulse. In the absorption spectra from excitation of ET and HET, the bands assignable to the DMB radical are obscured by broad bands in the 300–470 nm region. The absorption spectra are assigned to the T_1 states of ET and HET. The lifetimes of the T_1 states of ET and HET were determined to be 3.0 ± 0.7 and 2.0 ± 0.6 μs, respectively. The absorption spectra of the T_1 states of ET and HET are comparable to the spectrum of the T_1 state of benzene.[17] In the absorption spectrum from photolysis of CET, three bands appear at 271, 307, and 321 nm. The absorption spectrum is assigned to the DMB radical, since substituted benzyl radicals are formed by C–X bond fission (X = Cl, Br).[6,9,10,14–16] The absorption intensity of the DMB radical decayed at 100 μs. The observation of the absorption spectrum of the DMB radical is consistent with that of the fluorescence spectra in Fig. 1. The absorption spectrum of the DMB radical has some resemblance to the spectra of the benzyl[14,16] and *p*-methylbenzyl[14,16,18] radicals.

3.2. Quantum yields for dissociation pathways

The quantum yields for the DMB radical were estimated from dissociation of ET and HET as follows. (1) The ratio of the DMB yields from dissociation of ET, HET, and CET was measured by comparing its fluorescence intensities on excitation at 308 nm after photolysis at 266 nm. (2) The DMB yield from dissociation of CET was measured by comparison of its absorbance with the naphthalene triplet absorbance as the standard on excitation at 266 nm. The absorption coefficient for the DMB radical is assumed to be 7.4×10^3 dm^3 mol^{-1} cm^{-1} (321 nm) from the value for the *p*-methylbenzyl radical.[18] Care must be taken as an assumption of the absorption coefficient may lead to a different estimation of the

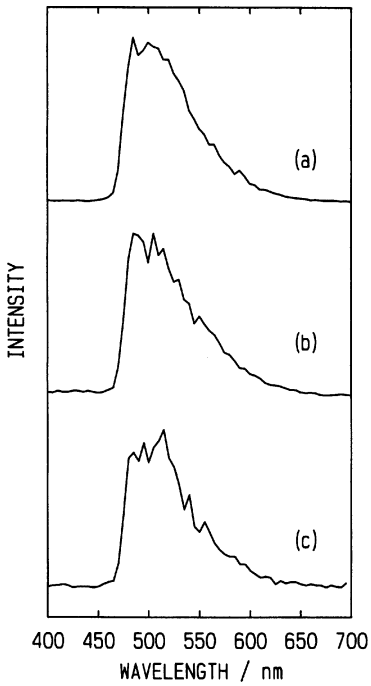

Fig. 1 Nanosecond fluorescence spectra of a DMB radical observed by excitation with a 308 nm pulse at 1 μs after excitation of (a) ET, (b) HET and (c) CET with a 266 nm pulse.

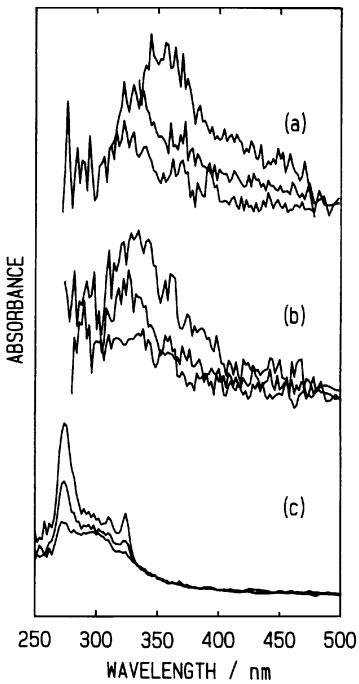

Fig. 2 Transient absorption spectra of a DMB radical observed after excitation of (a) ET, (b) HET and (c) CET with a 266 nm pulse. Delay time (from upper to lower curve): (a) 1, 5, 100; (b) 1, 5, 100; (c) 1, 10, 50 μs.

quantum yields. The absorption coefficient for the naphthalene triplet is 1.4×10^4 dm^3 mol^{-1} cm^{-1} (415 nm),[19] and the intersystem crossing yield for naphthalene is 0.68.[19] In this way, an estimate for the DMB yields of 4.2×10^{-3}, 1.7×10^{-3}, and 0.13 is made, respectively, from dissociation of ET, HET, and CET. The dissociation channels of the CH–H bond for ET and of the CH–OH bond for HET are shown to be small channels.

3.3. Dissociation rates

To elucidate excited states leading to dissociation, the rise rates of the DMB radical were compared with the decay rates of the S_1 states of ET and HET. For the ground state of the radical, the rise rates were determined from the dependence of its fluorescence intensity on the delay from the 266 nm (photolysis) to the 308 nm (probe) pulse. The jitter of the 266 nm pulse was limited to <0.5 ns, while the delay of the 308 nm pulse was calibrated with the photodiode signal. With respect to thermally equilibrated levels of the S_1 states of the precursors, the decay rates were measured from their fluorescence intensity-time profiles.

The fluorescence intensity–time profiles of ET and HET, observed by excitation with the 266 nm pulse, are shown in Fig. 3(a) and (c). The decay rates are determined to be $(4.0 \pm 1.0) \times 10^7$ s^{-1} for the ET fluorescence and $(4.5 \pm 0.6) \times 10^7$ s^{-1} for the HET fluorescence.

The dependence of the fluorescence intensity of the DMB radical on the delay of the 308 nm pulse, recorded by photolysis of ET with the 266 nm pulse, is shown in Fig. 3(b). The DMB fluorescence begins to rise at a 0 ns delay of the 308 nm pulse and reaches a plateau at a 60 ns delay of this pulse. The rise rate of the DMB fluorescence is equal to the decay rate of the ET fluorescence, and no rapid rise component exists in the rise process of the DMB fluorescence. The delay dependence of the DMB fluorescence intensity can be simulated satisfactorily with a rise rate of 4.0×10^7 s^{-1} for the DMB radical, which is equal to the decay rate for the ET fluorescence. This shows that the dissociation channel of the CH–H bond for ET takes place *via* thermally equilibrated levels of the S_1 state after vibrational relaxation.

The dependence of the fluorescence intensity of the DMB radical on the delay of the 308 nm pulse, recorded by photolysis of HET with the 266 nm pulse, is shown in Fig. 3(d). The DMB fluorescence begins to rise at a -10 ns delay of the 308 nm pulse and the intensity rise is almost completed at a 10 ns delay of this pulse. The rise rate of the DMB fluorescence is much faster than the decay rate of the HET fluorescence. Simulation with a rise rate of 4.5×10^7 s^{-1} for the DMB radical, a value equal to the decay rate for the HET fluorescence, cannot reproduce the delay dependence of the DMB fluorescence intensity. Instead, a rise rate of $>1.0 \times 10^9$ s^{-1} for the DMB radical is found to be necessary to simulate the experimental result. This shows that the major part of the dissociation channel of the CH–OH bond for HET takes place from vibrationally excited levels of the S_1 state in competition with vibrational relaxation. A minor fraction ($\sim$1/10) of the DMB fluorescence seems to rise in a 40 ns delay. Whether the slow rise rate corresponds to the decay rate of the HET fluorescence or not cannot be determined. This does not preclude the possibility that a minor part of the dissociation channel of the CH–OH bond for HET exists *via* thermally equilibrated levels of the S_1 state.

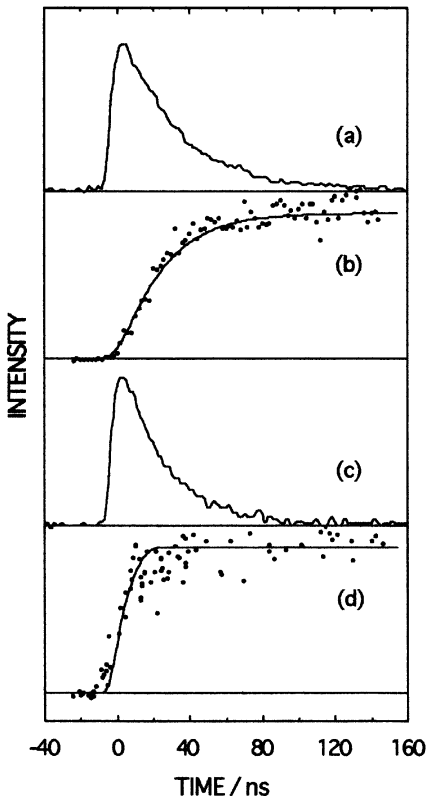

Fig. 3 Time evolution of fluorescence intensities of (a) ET and (c) HET recorded after excitation with a 266 nm pulse. Dependence of the fluorescence intensity of (b), (d) a DMB radical on the delay time from a 266 to a 308 nm pulse. Fluorescence of a DMB radical is induced by excitation with a 308 nm pulse after excitation of (b) ET and (d) HET with a 266 nm pulse. Monitoring wavelength: (a), (c) 300; (b), (d) 500 nm.

3.4. One- or two-photon photochemistry

The number of photons required for excitation of ET and HET to their dissociative states was determined from the dependence of the fluorescence intensity of the DMB radical on the fluences of the 266 nm (photolysis) and 308 nm (probe) pulses. Beer's law complication was removed at the dilute radical concentration ($<10^{-2}$ absorbance). A rough estimate for the probabilities that the S_1 and D_0 states were excited into higher states was made on the basis of the following absorption coefficients: 4.2×10^3 dm^3 mol^{-1} cm^{-1} (266 nm) for the S_1 states of ET and HET assumed from the value for benzene;[17] 2.4×10^3 dm^3 mol^{-1} cm^{-1} (266 nm) and 3.7×10^3 dm^3 mol^{-1} cm^{-1} (308 nm) for the D_0 state of the DMB radical taken from the values for the *p*-methylbenzyl radical.[18]

The logarithmic plots of the fluorescence intensity of the DMB radical *vs.* the 266 nm pulse fluence are shown for dissociation of ET and HET in Fig. 4(a) and (c). The probabilities of $S_n \leftarrow S_1$ excitation with the 266 nm pulse at its highest fluences are estimated to be 0.064 (6.1 mJ cm^{-2}) for ET and 0.091 (8.8 mJ cm^{-2}) for HET. The probability of $D_1 \leftarrow D_0$ excitation with the 266 nm pulse is negligible for dissociation of ET, because the major portion of the radicals are formed gradually after excitation of the precursors with this pulse. The probability of $D_1 \leftarrow D_0$ excitation is calculated to be 0.053 (8.8 mJ cm^{-2}) for dissociation of HET, if formation of the radicals occurs immediately after absorption of a 266 nm photon by the precursors. Observed points are linearly fitted with slopes of 1.04 ± 0.10 and 1.00 ± 0.06 for dissociation of ET and HET, respectively. It is clear that dissociation proceeds by 266 nm one-photon excitation.

The DMB fluorescence intensity is plotted as a function of the 308 nm pulse fluence for dissociation of ET and HET in Fig. 4(b) and (d). The probabilities of $D_1 \leftarrow D_0$ excitation with the 308 nm pulse at its highest fluences are estimated to be 0.24 (11 mJ cm^{-2}) for dissociation of ET and 0.46 (21 mJ cm^{-2}) for dissociation of HET. Linear fitting results in slopes of 1.10 ± 0.08 and 0.91 ± 0.11 for dissociation of ET and

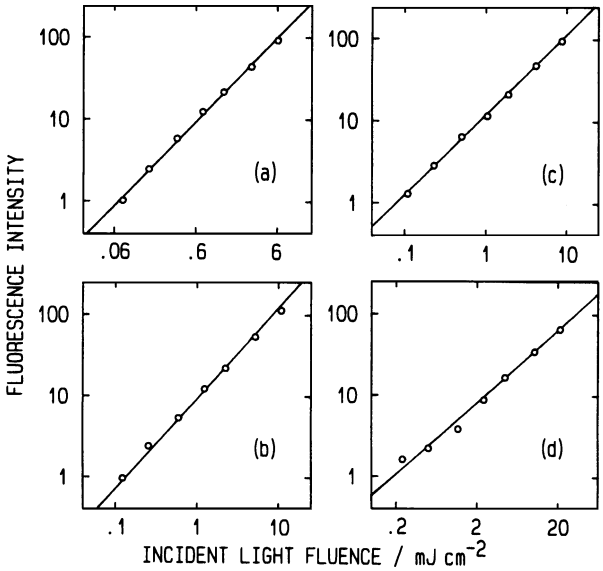

Fig. 4 Dependence of the fluorescence intensity of a DMB radical on (a), (c) 266 and (b), (d) 308 nm pulse fluences. Fluorescence is induced by excitation with a 308 nm pulse at 1 μs after excitation of (a), (b) ET and (c), (d) HET with a 266 nm pulse. Monitoring wavelength: 500 nm.

HET, respectively. It is evident that one 308 nm photon is required to populate the fluorescent state of the radical.

4. Discussion

4.1. Bond dissociation energies

Dissociation of ET and HET follows one-photon excitation to the S_1 states at 266 nm (Section 3.4). Excitation with one 266 nm photon (37 600 cm^{-1}) populates the S_1 states of ET (v_0 = 36 400 cm^{-1}) and HET (v_0 = 36 600 cm^{-1}) with excess vibrational energies. The bond dissociation energies are estimated for $C_6H_5CH(CH_3)$–H (29 400 cm^{-1}) and $C_6H_5CH(CH_3)$–OH (28 500 cm^{-1}) from the values given below: $C_6H_5CH_2$–H (30 700 cm^{-1}), CH_3CH_2–H (35 000 cm^{-1}), $(CH_3)_2CH$–H (33 700 cm^{-1}), $(CH_3)_2CH$–OH (32 800 cm^{-1}).[20] The energies that ET and HET possess are sufficient to cleave, respectively, the CH–H bond of the CH_2 group and the CH–OH bond of the CH(OH) group. Dissociation takes place by CH–H bond fission in ET and by CH–OH bond fission in HET (Section 3.1).

4.2. Potential energy surfaces

For ET, dissociation of the CH–H bond of the CH_2 group takes place ($\sim 10^{-3}$ yield) *via* thermally equilibrated levels of the S_1 state (Sections 3.2 and 3.3). For HET, dissociation of the CH–OH bond of the CH(OH) group occurs ($\sim 10^{-3}$ yield) from vibrationally excited levels of the S_1 state (Sections 3.2 and 3.3). The difference in the dissociation pathways between the CH–H and CH–OH bonds can be understood by the symmetries of the potential energy surfaces along the reaction coordinates.[11,12,21–27]

The most favorable geometry of CH–H and CH–OH bond stretch that leads to the planar benzyl radical is one in which it occurs in the symmetry (C_s) plane perpendicular to the benzene rings (see Fig. 5). The energy of this geometry is comparable to that of other geometries of CH–H and CH–OH bond stretch, even if they are distorted by vibrations. Thus, the approximation is made that the CH–H and CH–OH bond fission coordinates lie in the symmetry (C_s) plane perpendicular to the benzene rings. The symmetries of the potential energy surfaces are noted with respect to the symmetry (C_s) plane. In ET and HET, the S_1 [$^1B_{2u}$, $\pi\pi^*$(benzene)] states are of A'' symmetry, and the T_1 [$^3B_{1u}$, $\pi\pi^*$(benzene)] states are of A' symmetry. The $\sigma\sigma^*$(C–H) repulsive (singlet and triplet) states of ET possess A' symmetry and the np(O)σ^*(C–O) repulsive (singlet and triplet) states of HET possess A'' symmetry, when the O–H bond lies in the symmetry (C_s) plane. The $\sigma\sigma^*$(C–H) ($v_0 \sim$ 65 000 cm^{-1}) and np(O)σ^*(C–O) ($v_0 \sim$ 55 000 cm^{-1}) singlet states correspond to the lowest excited states in alkanes and alkyl alcohols, respectively. In the DMB radical, the D_0 ($^2B_2$) state is of A' symmetry, and the D_1 ($^2A_2$) state is of A'' symmetry.[28] The symmetry of the D_0 (^2S) state H atom is A', and the symmetry of the D_0 ($^2\Pi$) state OH radical is $A' + A''$.

For dissociation of ET, the S_1 (A'') state of the precursor does not correlate adiabatically to the ground ($^2B_2 + {}^2S$, A') state of the asymptotic products. Owing to the symmetry-imposed barrier, CH–H bond fission does not take place adiabatically from the S_1 state. It is allowed to occur by intersystem crossing to the T_1 state,[12] where crossing between the $\pi\pi^*$(benzene) (T_1, A') and $\sigma\sigma^*$(C–H) (A') configurations is

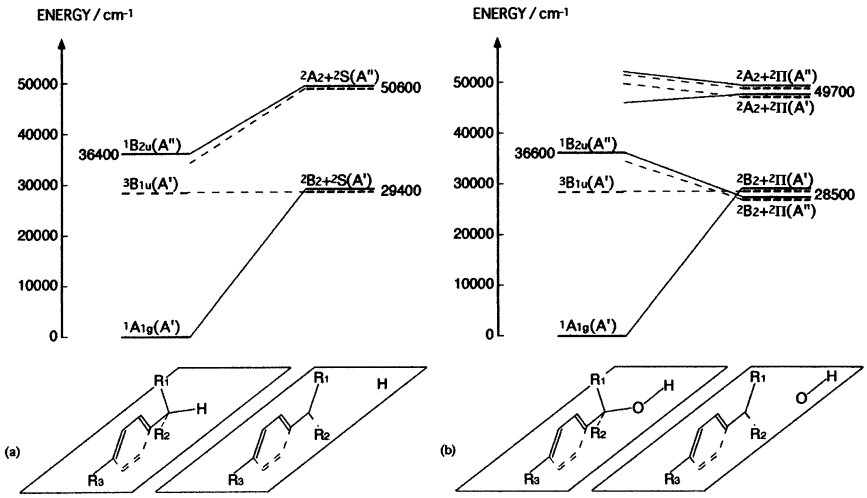

Fig. 5 State correlation diagrams (a) for CH–H bond fission of ET and (b) for CH–OH bond fission of HET. States of (a) ET and (b) HET are represented with the corresponding states of benzene (D_{6h}), and states of a DMB radical with those of a benzyl radical (C_{2v}). Symmetry representations relative to a symmetry plane are noted for singlet (solid lines) and triplet (broken lines) states in parentheses. Benzene rings are perpendicular to a symmetry plane, on which (a) CH–H and (b) CH–OH bonds lie. R_1 = H; R_2 = R_3 = CH_3.

avoided. In the liquid phase, intersystem crossing cannot compete with vibrational relaxation, and CH–H bond fission follows vibrational relaxation. This predicts that the dissociation rate is limited by the decay rate of thermally equilibrated levels of the S_1 state. Dissociation actually occurs from vibrationally-excited levels of the T_1 state, and the low dissociation yield ($\sim 10^{-3}$) is expected by competition with vibrational relaxation ($\sim 10^{11}$ s^{-1} rate) in the T_1 state.

The dissociation mechanism is similar to that of the C–X bonds (X = Cl, Br) for 1- and 2-(halomethyl)naphthalene excited to the S_2 states at 266 and 299 nm in the liquid phase.[29,30] For these molecules, dissociation takes place by intersystem crossing to upper triplet states which are themselves, or cross to, the σσ* dissociative triplet states, and is not affected by the amounts of excess vibrational energies (4 900 and 700 cm^{-1}).

For dissociation of HET, avoided crossing takes place between the ππ*(benzene) (S_1, A'') and np(O)σ*(C–O) (A'') configurations at the geometry of the stretched CH–OH bond. It provides the A'' adiabatic potential energy surface, which has ππ*(benzene) character in the Franck–Condon region but evolves to np(O)σ*(C–O) character beyond the barrier along the CH–OH bond fission coordinate. Rapid CH–OH bond fission occurs directly on the A'' adiabatic potential energy surface from the S_1 state of the precursor to the ground ($^2B_2$ + $^2\Pi$) state of the asymptotic products. This accounts for the dissociation pathway that occurs from vibrationally excited levels of the S_1 state. The low dissociation yield ($\sim 10^{-3}$) is explained by competition with vibrational relaxation ($\sim 10^{11}$ s^{-1} rate) in the S_1 state. There will be a higher probability for CH–OH bond fission, if the precursor possesses a large vibrational energy, *i.e.*, if it is pumped into highly vibrationally excited levels of the S_1 state.

4.3. Molecular geometry

The photon energy is absorbed initially by the benzene system, and electronic excitation is localized on it. The energetically available ground state of the product radical has no ππ*(benzene) character. Hence, considerable electronic rearrangement must be involved in dissociation. CH–H and CH–OH bond fission is possible, if an electronic change occurs in the respective bonds during dissociation. This may be enabled in the geometry which leads to potential coupling to the σσ*(C–H) and np(O)σ*(C–O) configurations.

The geometry is described by internal rotations about the C_6H_4–CH_2CH_3, C_6H_4–$CH(OH)CH_3$ and CH–OH bonds and by π hydrogen-bonding between the benzene system and OH group. These interactions are assumed from those of related molecules.

(1) For *p*-fluorotoluene, the CH_3 group undergoes nearly free internal rotation about the C_6H_4–CH_3 bond.[31] The barriers to internal rotation are 4.8 cm^{-1} in the S_0 state and 33.7 cm^{-1} in the S_1 state. For ET and HET, internal rotation may be nearly free about the C_6H_4–CH_2CH_3 and C_6H_4–$CH(OH)CH_3$ bonds, respectively.

(2) For ethanol, the OH group experiences highly hindered internal rotation about the CH_2–OH bond.[32] The conformation is least stable when the H atom of the OH group is eclipsed by the CH_3 group. The energy differences are 408.7 cm^{-1} between the eclipsed and *gauche* conformations and 452.0 cm^{-1} between the eclipsed and *trans* conformations in the S_0 state. For HET, highly hindered OH internal rotation may occur about the CH–OH bond.

(3) For the benzene–methanol cluster, the π hydrogen-bond is formed when the H atom of the OH group is donated to the delocalized π cloud of the benzene system.[33,34] The methanol molecule is pulled off the six-fold axis of the benzene ring, and the H atom of the OH group is nearly on the C atom of the benzene plane. The distance from the O atom to the benzene plane is 3.41 Å, and the binding energy is 1 680 cm^{-1} in the S_0 state. For HET, the H atom of the OH group may be π hydrogen-bonded to the π cloud of the benzene system. The distance between the H atom of the OH group and the C atom of the benzene ring adjacent to the CH(OH) group is estimated to be 2.35 Å from the following values: C_6H_4–C (1.52 Å),[35] C–O (1.43 Å),[36,37] O–H (0.94 Å),[36] C–C–O (111°),[37] C–O–H (110°).[36]

By intersystem crossing from the S_1 state (v_0 = 36 400 cm^{-1}) to the T_1 state (v_0 = 28 900 cm^{-1}), ET gains an excess vibrational energy (7 500 cm^{-1}) corresponding to the energy gap between the S_1 and T_1 states. If the excess energy is distributed over the 60 vibrational modes including the CH–H bond stretch mode, vibrational excitation is characterized by a high vibrational temperature (~580 K). If a larger part of the excess energy is distributed to the CH–H bond stretch mode, or if the excess energy is relaxed among the vibrational quanta, vibrational excitation of the 59 modes other than the CH–H bond stretch mode is equivalent to a somewhat lower vibrational temperature. Since internal rotation is nearly free about the C_6H_4–CH_2CH_3 bond, the conformation where the CH–H bond lies in the symmetry (C_s) plane perpendicular to the benzene ring is as stable as the other conformations. There will exist a probability that the CH–H bond lies in the symmetry (C_s) plane for the T_1 state.

In order to cross the barrier to CH–H bond fission, the molecule must undergo intersystem crossing to the T_1 state.[12] The electronic wave function must change subsequently from the ππ*(benzene) (T_1) to the σσ*(C–H) configuration. Also, the adiabatic potential energy surfaces must be split at the barrier to CH–H bond fission. When the CH–H bond lies in the symmetry (C_s) plane perpendicular to the benzene ring, the two configurations are symmetric relative to this plane. Splitting is represented, by configuration mixing, with the exchange interaction matrix element of the form:

$$K = \langle \pi^*_{\text{benzene}}(2)\sigma_{\text{C–H}}(1)(e^2/r_{12})\pi_{\text{benzene}}(1)\sigma^*_{\text{C–H}}(2)\rangle. \qquad (3)$$

The overlap integral is ignored. The π_{benzene} and π^*_{benzene} orbitals are made up of six p_{Ci} atomic orbitals of the benzene system. The p_{Ca} atomic orbital of the benzene system adjacent to the CH_2 group possesses a considerable electron density p^2_{Ca}. The p_{Ca} orbital is at a short distance from the $\sigma_{C–H}$ and $\sigma^*_{C–H}$ orbitals, and has overlap densities $p_{Ca}\sigma_{C–H}$ and $p_{Ca}\sigma^*_{C–H}$ with them. The exchange interaction matrix element may arise from these overlap densities. The $\sigma_{C–H}$ and $\sigma^*_{C–H}$ orbitals are in the direction of the CH–H bond, and the overlap densities and exchange interaction matrix element depend on the orientation of this bond. When the CH–H bond lies in the symmetry (C_s) plane, *i.e.*, when the $\sigma_{C–H}$ and $\sigma^*_{C–H}$ orbitals are in the same plane as the p_{Ca} orbital, the exchange interaction matrix element will have a maximum. This will allow potential coupling between the ππ*(benzene) and σσ*(C–H) configurations, and will permit the electronic wave function to change to the σσ*(C–H) configuration, thereby providing the probability of CH–H bond fission.

After excitation to the S_1 state (v_0 = 36 600 cm^{-1}) with a 266 nm photon (37 600 cm^{-1}), HET possesses an excess vibrational energy (1 000 cm^{-1}). Part of the excess energy may be distributed to local excitation of the CH–OH bond stretch mode. If the excess energy is distributed over the 60 vibrational modes including the CH–OH bond stretch mode, vibrational excitation corresponds to a low vibrational temperature (~350 K). Since internal rotation is nearly free about the C_6H_4–$CH(OH)CH_3$ bond, the conformation where the CH–OH bond lies in the symmetry (C_s) plane perpendicular to the benzene ring is as stable as the other conformations. Because internal rotation is highly hindered about the CH–OH bond, the *trans* conformation is more stable and the eclipsed conformation is less stable between the benzene ring and OH group. However, the eclipsed conformation may be

stabilized by π hydrogen-bonding between the benzene system and OH group. As a result, the probability will be high that the CH–OH and O–H bonds lie in the symmetry (C_s) plane for the S_1 state.

For CH–OH bond fission to occur in the S_1 state, the electronic configuration must change from being localized on the benzene (S_1, ππ*) system to being associated with the C–O (npσ*) bond. When the CH–OH and O–H bonds lie in the symmetry (C_s) plane perpendicular to the benzene ring, the ππ*(benzene) (S_1) and np(O)σ*(C–O) configurations are antisymmetric relative to this plane. Splitting between the adiabatic potential energy surfaces at the barrier to CH–OH bond fission is described with the Coulomb and exchange interaction matrix elements:

$$J' = \langle \pi^*_{\text{benzene}}(1) \text{np}_\text{O}(2) (e^2/r_{12}) \pi_{\text{benzene}}(1) \sigma^*_{\text{C–O}}(2) \rangle, \quad (4)$$

$$K' = \langle \pi^*_{\text{benzene}}(2) \text{np}_\text{O}(1) (e^2/r_{12}) \pi_{\text{benzene}}(1) \sigma^*_{\text{C–O}}(2) \rangle. \quad (5)$$

The Coulomb, and possibly exchange, interaction matrix elements will have finite values, since the CH–OH bond is not remote from the benzene system. Then, electron correlation will facilitate the change of the electronic wave function, and the nuclear dynamics will sample the trajectory towards the np(O)σ*(C–O) configuration, resulting in CH–OH bond fission.

5. Conclusion

After excitation to the S_1 states at 266 nm, ET dissociates by CH–H bond fission, and HET decomposes by CH–OH bond fission. CH–H bond fission of ET takes place *via* thermally equilibrated levels of the S_1 state, and CH–OH bond fission of HET occurs from vibrationally excited levels of the S_1 state. The observations are interpreted on a model of electron correlation between the precursor and product states in the geometry where the reaction coordinates lie in the symmetry plane perpendicular to the benzene rings.

References

1 N. Ikeda, N. Nakashima and K. Yoshihara, *J. Chem. Phys.*, 1985, **82**, 5285.
2 K. Tsukiyama and R. Bersohn, *J. Chem. Phys.*, 1987, **86**, 745.
3 Y. Kajii, K. Obi, I. Tanaka, N. Ikeda, N. Nakashima and K. Yoshihara, *J. Chem. Phys.*, 1987, **86**, 6115.
4 N. Nakashima, N. Ikeda and K. Yoshihara, *J. Phys. Chem.*, 1988, **92**, 4389.
5 J. Park, R. Bersohn and I. Oref, *J. Chem. Phys.*, 1990, **93**, 5700.
6 U. Brand, H. Hippler, L. Lindemann and J. Troe, *J. Phys. Chem.*, 1990, **94**, 6305.
7 K. Luther, J. Troe and K.-M. Weitzel, *J. Phys. Chem.*, 1990, **94**, 6316.
8 H. Hippler, C. Riehn, J. Troe and K.-M. Weitzel, *J. Phys. Chem.*, 1990, **94**, 6321.
9 K. W. Haider, E. Migirdicyan, M. S. Platz, N. Soundararajan and A. Despres, *J. Am. Chem. Soc.*, 1990, **112**, 733.
10 J. L. Faria and S. Steenken, *J. Phys. Chem.*, 1993, **97**, 1924.
11 M. Fujiwara and K. Toyomi, *J. Chem. Phys.*, 1997, **107**, 9354.
12 M. Fujiwara, A. Yamasaki, K. Mishima and K. Toyomi, *J. Chem. Phys.*, 1998, **109**, 1359.
13 P. K. Chowdhury, *J. Phys. Chem.*, 1994, **98**, 13112.
14 K. Tokumura, M. Udagawa, T. Ozaki and M. Itoh, *Chem. Phys. Lett.*, 1987, **141**, 558.
15 D. Meisel, P. K. Das, G. L. Hug, K. Bhattacharyya and R. W. Fessenden, *J. Am. Chem. Soc.*, 1986, **108**, 4706.
16 K. Tokumura, T. Ozaki, H. Nosaka, Y. Saigusa and M. Itoh, *J. Am. Chem. Soc.*, 1991, **113**, 4974.
17 N. Nakashima, M. Sumitani, I. Ohmine and K. Yoshihara, *J. Chem. Phys.*, 1980, **72**, 2226.
18 R. F. C. Claridge and H. Fischer, *J. Phys. Chem.*, 1983, **87**, 1960.
19 I. Carmichael and G. L. Hug, in *CRC Handbook of Organic Photochemistry*, ed. J. C. Scaiano, CRC Press, Boca Raton, FL, 1989, vol. 1, ch. 16.
20 D. Griller and J. M. Kanabus-Kaminska, in *CRC Handbook of Organic Photochemistry*, ed. J. C. Scaiano, CRC Press, Boca Raton, FL, 1989, vol. 2, ch. 17.
21 L. Salem, *J. Am. Chem. Soc.*, 1974, **96**, 3486.
22 N. J. Turro, W. E. Farneth and A. Devaquet, *J. Am. Chem. Soc.*, 1976, **98**, 7425.
23 M. D. Person, P. W. Kash, S. A. Schofield and L. J. Butler, *J. Chem. Phys.*, 1991, **95**, 3843.
24 M. D. Person, P. W. Kash and L. J. Butler, *J. Chem. Phys.*, 1992, **97**, 355.
25 P. W. Kash, G. C. G. Waschewsky, L. J. Butler and M. M. Francl, *J. Chem. Phys.*, 1993, **99**, 4479.
26 P. W. Kash, G. C. G. Waschewsky, R. E. Morss, L. J. Butler and M. M. Francl, *J. Chem. Phys.*, 1994, **100**, 3463.
27 T. L. Myers, N. R. Forde, B. Hu, D. C. Kitchen and L. J. Butler, *J. Chem. Phys.*, 1997, **107**, 5361.
28 J. E. Rice, N. C. Handy and P. J. Knowles, *J. Chem. Soc., Faraday Trans. II*, 1987, **83**, 1643.
29 D. F. Kelley, S. V. Milton, D. Huppert and P. M. Rentzepis, *J. Phys. Chem.*, 1983, **87**, 1842.
30 E. F. Hilinski, D. Huppert, D. F. Kelley, S. V. Milton and P. M. Rentzepis, *J. Am. Chem. Soc.*, 1984, **106**, 1951.
31 K. Okuyama, N. Mikami and M. Ito, *J. Phys. Chem.*, 1985, **89**, 5617.
32 P. K. Kakar and C. R. Quade, *J. Chem. Phys.*, 1980, **72**, 4300.
33 A. W. Garrett, D. L. Severance and T. S. Zwier, *J. Chem. Phys.*, 1992, **96**, 7245.
34 R. N. Pribble, F. C. Hagemeister and T. S. Zwier, *J. Chem. Phys.*, 1997, **106**, 2145.
35 C. Bois, *Bull. Soc. Chim. Fr.*, 1966, 4016.
36 J. Hvoslef, *Acta Crystallogr.*, 1958, **11**, 383.
37 R. Shiono, D. W. J. Cruickshank and E. G. Cox, *Acta Crystallogr.*, 1958, **11**, 389.